Available online at www.sciencedirect.com

SCIENCE DIRECT

Journal of Electrocardiology 39 (2006) 290–297

JOURNAL OF Electrocardiology

www.elsevier.com/locate/jelectrocard

Atrial repolarization as observable during the PQ interval

Zenichi Ihara, MSc[a,*], Adriaan van Oosterom, PhD[b], Rudi Hoekema, PhD[c]

[a]*Signal Processing Institute, Swiss Federal Institute of Technology Lausanne (EPFL), CH-1015 Lausanne, Switzerland*
[b]*Department of Cardiology, Centre Hospitalier Universitaire Vaudois (CHUV), Switzerland*
[c]*Department of Cardiology, Radboud University Nijmegen Medical Centre, The Netherlands*

Received 15 August 2005; accepted 1 December 2005

Abstract

Objective: We aimed to study the involvement of atrial repolarization in body surface potentials.
Methods: Electrocardiograms of healthy subjects were recorded using a 64-lead system. The data analysis focused on the PQ intervals while devoting special attention to the low-amplitude signals during the PQ segment: the segment from the end of the P wave until onset QRS. The data were analyzed by inspecting body surface potential maps and the XYZ signals of the vectorcardiogram.
Results: Standard P-wave features exhibited normal values. The local potential extremes were found at positions not sampled by the standard leads. The PQ segment was found to be not isoelectric, the time course of the potential distribution being very similar to that during the P wave but for a reversed polarity and about 3-fold lower magnitudes.
Conclusion: The results demonstrate a significant involvement of atrial repolarization during the PQ interval and essentially discordant "atrial T waves," suggesting a small dispersion of atrial action potential durations.

Keywords: Atrial repolarization; P wave; ECG; VCG; PQ interval

Introduction

Measuring body surface potentials in the assessment of the electrical activity of the heart is the most commonly used, noninvasive method for diagnosing cardiac arrhythmias. The current clinical interest in the electrical activity of the atria, with its focus on atrial fibrillation (AF), has revealed the relatively scarce knowledge that is available concerning the information content of P-wave morphology. Within the context of attempting to fill in various gaps existing in the understanding of such waveforms, the present work investigated the involvement of atrial repolarization process during the PQ interval. This process is usually taken to coincide exclusively with, and thus masked by, the QRST complex. Because the amplitudes of the atrial signals observed on the thorax are of the order of 100 μV and considerably lower during the PQ segment, special attention was given to the preprocessing of the data, in particular, to the identification of the baseline. For this reason, the various steps taken are described in some detail.

Materials

Electrocardiograms (ECGs), simultaneously recorded by using a 64-lead system, were taken from 75 healthy volunteers (57 males, 18 females). The recruitment aimed at including a wide range of ages and constitutional variables.

The data comprise the recordings of 50 subjects (42 males, 8 females) (database, DB1[1]) observed using the "Nijmegen" lead system[2,3] and 25 subjects (15 males, 10 females) (database, DB2[4]) observed using the "Amsterdam" lead system.[3,5] The main statistics of the age of the subjects is shown in Table 1. The full specification of the constitutional variables of the subjects in DB2 was documented in Reference 6.

Physical examination of the subjects, including the measurement of blood pressure, analysis of the standard 12-lead ECG, echocardiography, and anamnesis, revealed no trace of any cardiac disorder. No hypertensives were included; left atrial dimensions were within normal limits.

The electrodes in both systems are distributed over the entire surface of the thorax, with a higher electrode density in the precordial region.[3] Both lead systems include the positions of the 9 electrodes of the standard 12-lead ECG, as well as the 7 electrodes of the Frank vectorcardiogram (VCG)[7] as subsets.

* Corresponding author. Tel.: +41 21 693 4754; fax: +41 21 693 7600.
E-mail address: zenichi.ihara@epfl.ch (Z. Ihara).

0022-0736/$ – see front matter © 2006 Elsevier Inc. All rights reserved.
doi:10.1016/j.jelectrocard.2005.12.001

Table 1
Basic statistics of age of the subjects studied, specified by sex and data base

	Age statistics (y)		
	Male	Female	All
DB1	42 (39.8 ± 15)	8 (43.0 ± 9.3)	50 (40.3 ± 14)
	(19.5, 41.3, 69.5)	(27.4, 46.1, 54.1)	(19.5, 42.6, 69.5)
DB2	15 (40.3 ± 14)	10 (33.8 ± 12)	25 (37.7 ± 13)
	(26.0, 34.2, 64.9)	(23.8, 29.1, 62.2)	(23.8, 33.4, 64.9)
ALL	57 (39.9 ± 15)	18 (37.9 ± 11.6)	75 (39.4 ± 14)
	(19.5, 35.7, 69.5)	(23.8, 36.1,62.2)	(19.5, 36.1, 69.5)

Values are presented as n (mean ± SD) (minimum, median, maximum).

For the subjects in DB1, the 64 signals were recorded simultaneously at a sampling rate of 500 samples per second (sps) with 2 μV resolution, using a hardware high-pass filter at 0.05 Hz. The signals of the 25 subjects in DB2 recorded with bandpass filter settings of 0.16 to 100 Hz and sampled at 1000 sps, with 0.7 μV resolution.[4] The recordings were made with the subjects at rest in the supine position; the mean heart rate of the subjects was 61.9 ± 8 (mean ± SD) beats per minute (range, 50-82 beats per minute; median, 62 beats per minute).

Methods

Definition of terms

The analysis of the atrial signals presented in this article relates to the entire depolarization and repolarization process of the atria. Because of this, rather than referring to signal components in individual leads, features were used that characterize the entire process. Their timing was extracted from the root-mean-square (RMS) curve, RMS(t), computed from all recorded lead signals, after application of the zero-mean reference. By denoting the potential of any individual lead, l, by $V_l(t)$, the function RMS(t) is defined as $\mathrm{RMS}(t) = \sqrt{\frac{1}{L}\sum_{\ell=1}^{L} V_\ell^2(t)}$, with L as the number of leads. This function is positive only; it provides an overall view of the depolarization and repolarization processes of the entire heart in a manner that is largely independent of the lead system used. An example of an RMS curve, computed from the 64-lead data of 1 subject, is shown in Fig. 1. As is shown by the dashed trace in Fig. 1A, it clearly identifies the onsets and end points of the P waves and QRS complexes of the subsequent beats. After application of the baseline correction described hereinafter (solid line), the quality of these markers is clearly enhanced.

Fig. 1B, an exploded view of the PQ interval of the RMS curve, is used to illustrate the definitions of the various terms used. The PQ interval is taken to be the interval between the timings t_{oP} and t_{oQ}, which denote the onset of atrial depolarization and that of ventricular depolarization, respectively. This interval is frequently, but imprecisely, referred to as the PR interval.[8] The maximum of the RMS curve is denoted by P_{apex}, its timing, by $t_{P_{apex}}$. The timing of the maximum curvature of the down slope of the RMS curve after P_{apex} is taken to signify the end of atrial depolarization. It is a time instant similar to that of the J point at the end of QRS. This moment is denoted by t_{Ja}. These time markers then define the duration of the P wave as the interval between t_{oP} and t_{Ja}. Finally, the interval from t_{Ja} to t_{oQ} is referred to as the PQ segment.

Processing the signals

The signals that had been sampled at 500 sps were up-sampled to 1000 sps by means of spline interpolation. This clearly facilitated their subsequent analysis. From the data set, for each subject, episodes of 10 seconds were selected showing a stable baseline in all of the lead signals. In about 1% of all of the recorded signals, this required a correction because of poor electrode contact. This correction was performed by using the method described by Oostendorp et al.[9]

Baseline correction

The times of the onsets of the P wave, t_{oP}, in all subsequent beats, were identified automatically from the RMS curve. These times were taken as markers indicating the smallest involvement of the ventricular electrical activity in the data observed on the thorax. Note that "the end of the T wave," estimated by whatever method, does not share this property. This poorly defined concept (the end of the T wave), supposedly characterizes the end of ventricular repolarization. The latter would mark the natural end point of any baseline correction. However, because such end points may be considerably affected by the presence of U waves, we used the latest available point: the onset of the next P wave.

Based on the observed values at the time instants t_{oP}, a spline-based automatic baseline correction was performed and applied individually to all of the 64 signals of each subject.

Selection of PQ segments

In the signals obtained after baseline correction, electric noise and muscle tremor artifacts were reduced by the application of a low-pass moving average filter taken over 20 samples, which has its first cutoff frequency at 50 Hz. The RMS curve of the filtered signals was used as an overall check of the previous processing steps. Next, this curve was used to identify the various timing makers described previously. The onset of atrial depolarization was taken to be t_{oP} as identified during the baseline correction procedure. The end of the PQ interval, t_{oQ}, was taken to be the time instant of the maximal curvature of the RMS curve in the time interval preceding the fast upstroke of the QRS-related part of the RMS curve. From the resulting PQ intervals, a single episode of the processed lead signals was used in the subsequent analysis. For each of the subjects, this resulted in a data matrix, $\mathbf{\Psi}$, of size 64 × NT, with NT as the number of samples, typically being 170 (milliseconds).

Vectorcardiogram derivation

The XYZ components of the VCG $\mathbf{V}$ were computed from the signals observed at the position of the 7 Frank electrodes by applying the coefficients of Frank's transfer matrix, $\mathbf{F}$[7]; hence, $\mathbf{V} = \mathbf{F\Psi}$. Matrix $\mathbf{V}$ has size 3 × NT; its 3 rows represent the signals $X(t)$, $Y(t)$, and $Z(t)$ of the vectorcardiogram.

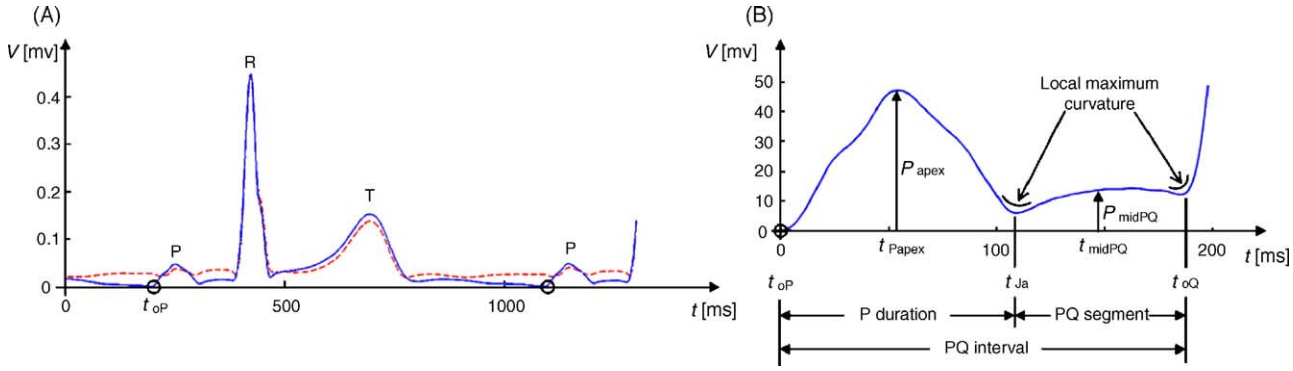

Fig. 1. Root-mean-square curves, derived from 64-lead data of one of the subjects, used for defining features and used in the various preprocessing steps. A, Dashed line indicates RMS curve derived after a crude initial baseline correction. Solid line indicates RMS curve after spline based baseline correction at the onsets (the circles) of the P waves in about 10 successive beats. B, Root-mean-square curve of the PQ interval, with an indication of the definition of the terms used.

Extracted features

The following features were extracted from the PQ segments.

From the RMS curve

The following features were selected from the RMS curve (see Fig. 1B).

PQ duration	$\mathrm{PQ}_{\mathrm{dur}} = t_{\mathrm{oQ}} - t_{\mathrm{oP}}$
P-wave duration	$P_{\mathrm{dur}} = t_{\mathrm{Ja}} - t_{\mathrm{oP}}$
Duration PQ segment	$\mathrm{PQ}_{\mathrm{seg}} = t_{\mathrm{oQ}} - t_{\mathrm{Ja}}$
Timing of apex	$t_{P_{\mathrm{apex}}}$
Amplitude of the apex	$P_{\mathrm{apex}} = \mathrm{RMS}(t = t_{P_{\mathrm{apex}}})$
Timing mid-PQ	$t_{\mathrm{mid\text{-}PQ}} = (t_{\mathrm{Ja}} + t_{\mathrm{oQ}})/2$
Amplitude halfway the PQ segment	$P_{\mathrm{mid\text{-}PQ}} = \mathrm{RMS}(t = t_{\mathrm{mid\text{-}PQ}})$

The choice of mid-PQ identifies a point in time where the depolarization of the atria may be considered as complete while also keeping well clear of the onset of depolarization of the ventricles.

From the 64-lead signals

For each subject, the leads were identified showing the maximal (positive) and the minimal (negative) potential values at $t = t_{P_{\mathrm{apex}}}$. The corresponding observed extremes are denoted by P^{+}_{apex} and P^{-}_{apex}, respectively. Similarly, the lead positions showing extreme potential values at $t = t_{\mathrm{mid\text{-}PQ}}$ were identified, as well as the corresponding extremes $P^{+}_{\mathrm{mid-PQ}}$ and $P^{-}_{\mathrm{mid-PQ}}$.

From the VCG

The $X(t)$, $Y(t)$, and $Z(t)$ components of the VCG were used to construct the signal $M(t)$ describing the time course of the spatial magnitude of the (P wave) vector: $M(t) = \sqrt{X^2(t) + Y^2(t) + Z^2(t)}$. The azimuth, elevation, and magnitude values of the vector at $t = t_{P_{\mathrm{apex}}}$ as well as at $t = t_{\mathrm{mid\text{-}PQ}}$ were added to the list of features. The azimuth and elevation were the conventional angles as used in vectorcardiography, φ and θ as shown in Fig. 3C, respectively.

Statistics

When possible, the observed features will be documented by their (mean ± SD) values, as well as their range. However, some of the features have the nature of directional data.[10] These are the locations of the leads exhibiting extreme potential values and the vector directions at the time instants $t = t_{P_{\mathrm{apex}}}$ and $t = t_{\mathrm{mid\text{-}PQ}}$.

Distribution of leads showing extreme potential values

The locations of leads showing extreme potential values were mapped on a standard geometry derived from the magnetic resonance imaging of the thorax of a male subject. The surface was made discrete by a triangular mesh comprising 364 nodes and 724 triangles. The nodes included the coordinates of the 64 leads of both the Amsterdam and the Nijmegen lead system. The number of times any individual node was identified as locating say P^{+}_{apex} was counted, resulting in lead specific values N_l ($0 \le N_l \le 75$). Because of the 2 different lead systems involved and the relatively low number of subjects (75), the method for displaying the distribution of these values over the thorax was not immediately obvious. We based the method used here on the Parzen estimators (see chapter 6 of Reference 11), now usually referred to as the Kernel Density Estimation.[12] It involves estimating a continuous density function from observed (discrete) data. To this end, an assumed basic density function (kernel) is centered at each observed data point and the estimated density is found by adding up the contributions of all of the resulting kernel functions. For our application to a closed surface, the kernel

Table 2
Basic statistics of timings and durations of 73 healthy subjects, derived from their RMS curves

	Durations and timings (ms)
PQ interval	170 ± 24 (122, 168, 285)
P duration	113 ± 13 (80, 113, 147)
PQ segment	57 ± 23 (10, 54, 176)
$t_{P_{\mathrm{apex}}}$	70 ± 13 (45, 72, 118)
$t_{\mathrm{mid\text{-}PQ}}$	146 ± 16 (113, 148, 201)

Values are presented as mean ± SD (minimum, median, maximum). Definitions as indicated in Fig. 1B.

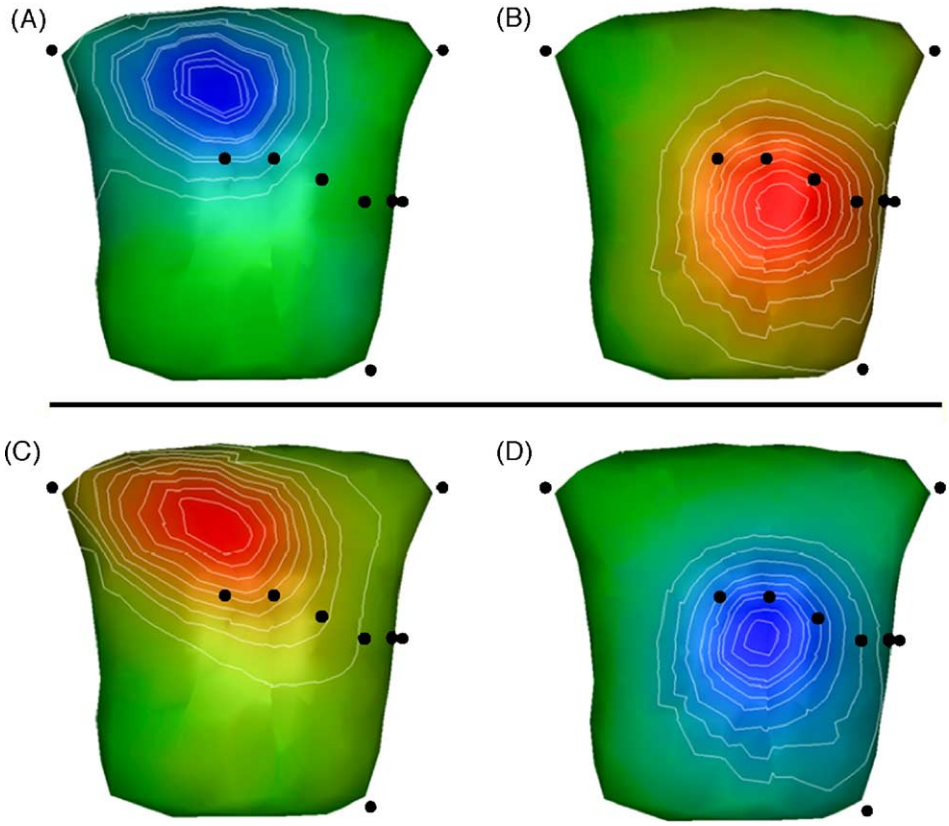

Fig. 2. Estimated densities of the location of the extreme potential values as observed in the 64-lead signals of 73 healthy subjects. The black dots indicate the locations of the 9 electrodes of the standard 12-lead ECG. Successive contour lines are drawn at increments of 10% of the total number of observations. A, Location of extreme negative values at $t = t_{P_{\text{apex}}}$. B, Location of extreme positive potentials at $t = t_{P_{\text{apex}}}$. C, Location of extreme positive potentials at $t = t_{\text{mid-PQ}}$. D, Location of extreme negative potentials at $t = t_{\text{mid-PQ}}$.

function chosen was the Gaussian distribution function, $f(d;\sigma) = \frac{1}{\sqrt{2\pi}\sigma} e^{-\frac{1}{2}(d/\sigma)^2}$, with d as the distance between an observed data point and the position where the function needs to be evaluated and σ as a parameter setting the shape of the kernel, which influences the spatial smoothness of the final result. The distance variable used was taken over the surface between any lead position showing an extreme potential value and any of the other nodes specifying the thorax geometry. The distances were computed by means of the shortest path algorithm applied to the individual edge lengths of the triangles.[13] The integral of the resulting density function over the entire surface was forced to be one. The resulting density function was studied by plotting its isofunction lines. These form demarcation lines of areas encompassing a given percentile of the observations, with increasing number of observations being enclosed as their contained area increases. The shape parameter was increased until individual "islands" around individual lead positions were no longer found.

Directional statistics

By their nature, the orientations of vectors in 3-dimensional space constitute directional data. The statistical handling of such data has been discussed extensively in the literature.[10,14] In the ECG literature, for the problem in hand, 2 statistics have been adopted from the general literature: the prevalent direction and the spatial precision.[15] These are measures similar to the mean and SD of single variates, respectively. By denoting the intersection of any vector $\vec{V}_i$ with a unit sphere by its components (x_i, y_i, z_i), the prevalent direction is that of the vector $(\bar{x}, \bar{y}, \bar{z})$, with the bars denoting the mean of the variables. The spatial precision is $\sqrt{\bar{x}^2 + \bar{y}^2 + \bar{z}^2}$, a variable having a range of 0 to 1, where 0 corresponds to a distribution randomly, uniformly scattered over a sphere, and 1 to the situation in which all samples are concentrated at the same coordinates. These statistics are used in the results section, where appropriate. However, as will be shown, the vectors around the prevalent direction are by no means distributed axially around this direction. Hence, the various statistical tests designed for this kind of problem cannot be applied.

Table 3
Basic statistics of the extreme potentials of 73 healthy subjects as observed on the 64 leads at times $t = t_{P_{\text{apex}}}$, the timing of the apex of the RMS curve, and $t = t_{\text{mid-PQ}}$, the timing of the middle of the PQ segment

	Potentials (μV)	
	$t_{P_{\text{apex}}}$	$t_{\text{mid-PQ}}$
Extreme positive value	55 ± 17	36 ± 13
	(22, 53, 133)	(8, 35, 70)
Extreme negative value	−93 ± 33	−33 ± 13
	(−189, −93, −34)	(−76, −31, −16)
Max difference	148 ± 45	69 ± 23
	(70, 147, 288)	(25, 68, 138)

Values are presented as mean ± SD (minimum, median, maximum). See Fig. 1B.

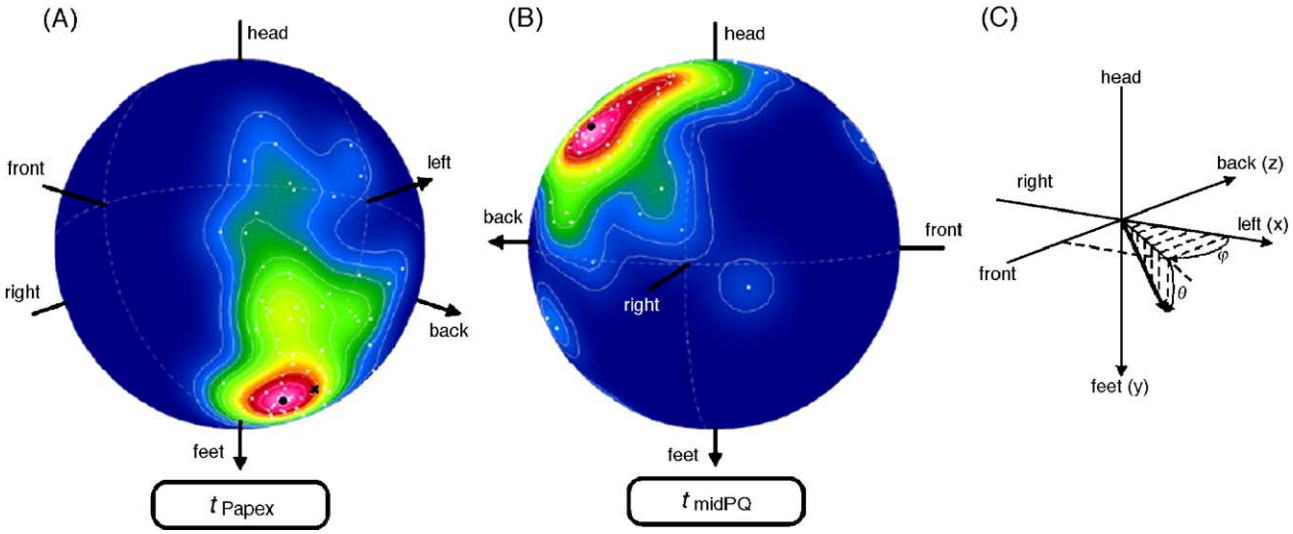

Fig. 3. Directional representation of the dipole source orientations. A, Dipole vector directions during atrial depolarization at $t = t_{P_{apex}}$. The white dots indicate the individual vector directions of 73 healthy subjects. The color map is the estimated continuous density. Increments of 10% between successive density lines. The large black dot indicates the position of the mode of the density, and the cross is the direction presented in the literature.[15] B, As in Fig. 3A, but now during repolarization at $t = t_{\text{mid-PQ}}$. C, Definition of the vector axes and the vector angles: azimuth φ and elevation θ.

Instead, density functions will be shown, drawn on a unit sphere, the kernel function now being the von Mises distribution function[10] $M(\theta;\kappa) = p_\kappa e^{\kappa\cos\theta}$, with θ as the angle between the 2 vectors specifying the observed vector direction and any other point on the unit sphere; κ, a shape parameter; and p_κ, a scaling parameter that was used while forcing the integral of the final overall estimated density to be one.

Results

When inspecting the raw ECG data, 2 cases were in DB1 that showed an insufficient signal-to-noise ratio in view of the low-level P-wave potentials. In DB2, 1 case was noted in which the data were recorded during a period of P-wave inversion. These 3 cases were excluded from the subsequent statistical analyses; their exclusion did not produce any significantly different change in any of the statistics.

From the RMS curve

The PQ intervals and the P-wave durations were found to have the same orders of magnitude as those previously presented in, for example, References 16,17. However, in contrast to what is perceived when comparing the results of those studies, no sex differences were observed in our data. An overview of the statistics of the features derived from the RMS curve is shown in Table 2.

From the 64-lead signals

The observed locations of extreme potential values are displayed in Fig. 2 by means of the density maps drawn on the anterior thorax. The shape parameter σ of the Gaussian kernel used for the Kernel Density Estimation was 8 cm. The black dots represent the locations of the 9 electrodes of a standard 12-lead ECG. At $t = t_{P_{apex}}$, the extreme positive potentials were observed in the region below the V_2 lead position (Fig. 2B); the accompanying extreme negative values were observed in the upper right chest. At $t = t_{\text{mid-PQ}}$, approximately the same regions were found, now for extremes having a reversed polarity. These extreme potential values, observed at the respective time instants, are documented in Table 3.

From the VCG

In Fig. 3, the directions of the observed dipole source vectors at $t = t_{P_{apex}}$ and $t = t_{\text{mid-PQ}}$ are shown, plotted on a unit sphere by means of their estimated density. The shape parameter κ of the von Mises density function, a dimensionless factor, was set at 50. The corresponding vector magnitudes and directions are presented in Table 4. The axes labeling used was according to the standard VCG display convention shown in Fig. 3C.[8,15] Fig. 3A shows a main dipole vector at $t = t_{P_{apex}}$ that is directed from the back of the right shoulder to the left leg. As shown in Fig. 3B, at

Table 4
Basic statistics of the vector data at times $t = t_{P_{apex}}$, the timing of the apex of the RMS curve, and $t = t_{\text{mid-PQ}}$, the timing of the middle of the PQ segment

	$t_{P_{apex}}$	$t_{\text{mid-PQ}}$
Vector magnitude (μV)	96 ± 32 (40, 92, 209)	30 ± 14 (5, 30, 86)
Prevalent direction (°)	$\varphi = 9$, $\theta = 50$	$\varphi = -132$, $\theta = -45$
Spatial precision	0.84	0.75
Angle of corresponding dispersion cone (°)	33	41
Angle between the prevalent directions at the 2 time instants (°)	135	
Spatial precision	0.90	
Angle of corresponding dispersion cone (°)	26	

The azimuth φ and elevation θ angles of the vectors are as defined in Fig. 3.

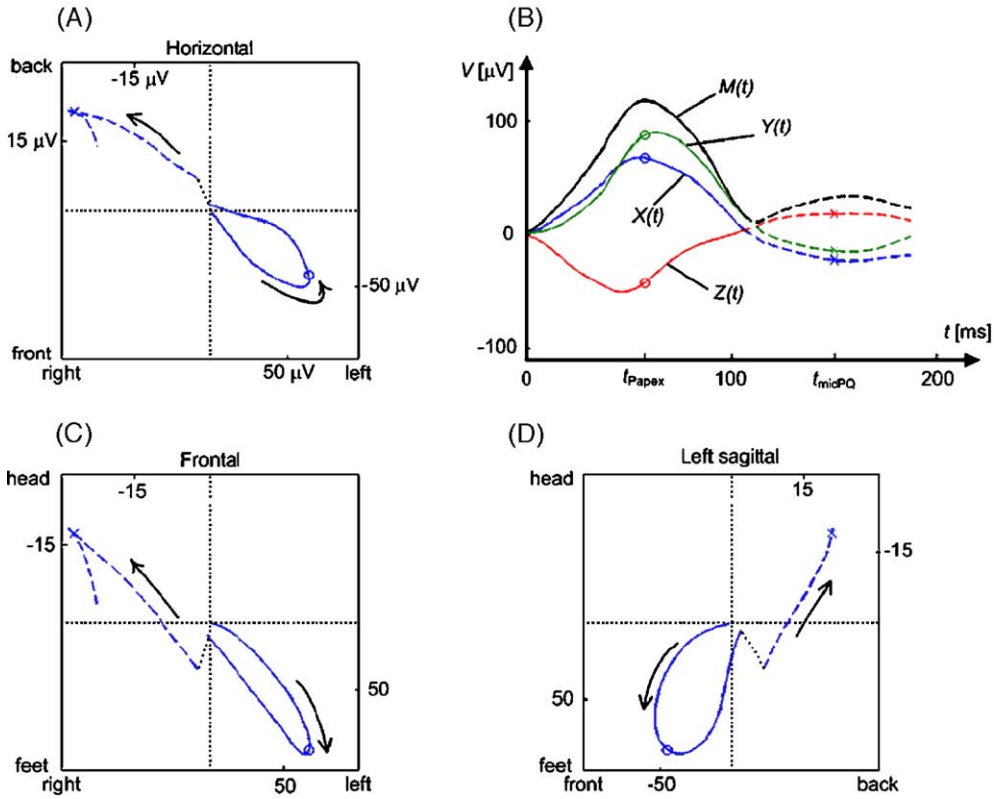

Fig. 4. Example of the vector data during the PQ interval (duration, 187 milliseconds) in one of the subjects. The trajectory of the vector displayed in 3 planes: horizontal (A), frontal (C), and left sagittal (D). The solid line is used during the duration of the P wave, whereas the dashed line represents the PQ segment, drawn to a different amplitude scale. The corresponding amplitude scales are expressed in microvolts. The circles indicate the instant of $t = t_{P_{apex}}$; the crosses indicate $t = t_{mid\text{-}PQ}$. B, The vector magnitude $M(t)$ and its components $X(t)$, $Y(t)$, and $Z(t)$. The PQ segment is shown in dashed lines, drawn to the same scale.

$t = t_{mid\text{-}PQ}$, the main vector showed an approximately reverse direction. The spatial orientation of P_{apex} presented in the literature[16] for males is indicated by a black cross in Fig. 3A, which lies within the density contour of 20%.

An example of the vector data of 1 subject during the PQ interval (187 milliseconds) is presented in Fig. 4. As shown in this figure, the vector loops of all subjects during the P wave revealed maximal values of the spatial magnitude $M(t)$ at time instants that were close to $t_{P_{apex}}$. Most of the loops in the horizontal plane (88%) had counterclockwise orientations such as the one shown in Fig. 4A. A similar result was found in the left sagittal plane, 92% having the counterclockwise orientation such as the one shown in Fig. 4D. By contrast, in the frontal plane, the orientation of the loop was less uniform: 28% revealed a clockwise orientation such as the one shown in Fig. 4C.

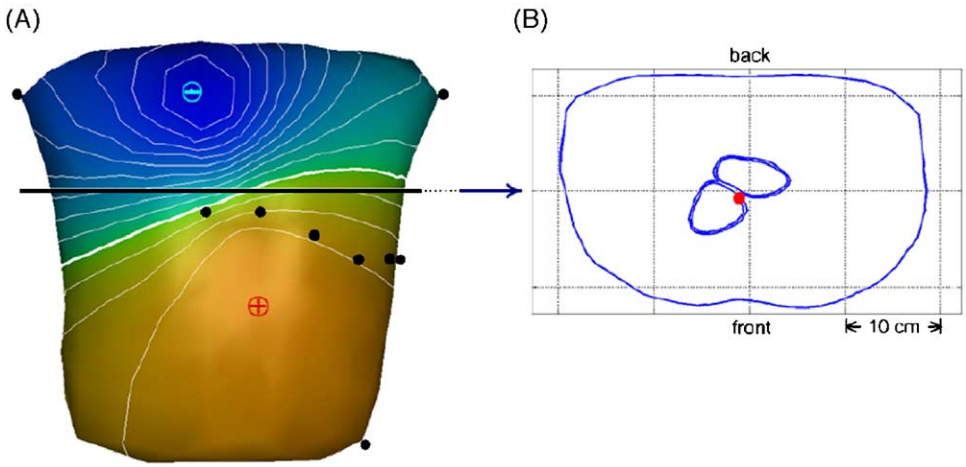

Fig. 5. A, Body surface map of the potential generated by a dipole with magnitude proportional to the mean vector at $t = t_{P_{apex}}$ (top row of Table 4) and having the corresponding prevalent direction (second row of Table 4) located inside a homogeneous thorax-shaped volume conductor. B, Location of the dipole (heavy dot) indicated in a cross section of the thorax. The heavy dots indicate the locations of the electrodes of the standard 12-lead ECG. The level of the cross section is at the center of gravity of the myocardial mass of the atria, whose outline is indicated. The level is indicated by the heavy black line in panel A. Isopotential lines in panel A drawn at 10 μV intervals, with the heavy line denoting zero with respect to the zero-mean thorax potential reference.

Because of the onset of ventricular depolarization, the vector loops related to the "atrial T waves" cannot be followed to their conclusion. However, those parts visible, as the one shown in Fig. 4, generally showed directions that were opposite to those of the mean vectors during the P wave. The magnitudes after $t_{\text{mid-PQ}}$ tended toward lower values.

Discussion

The characteristics of the observed P waves are in agreement with those previously described in the literature.[18] To these characteristics, owing to some dedicated preprocessing steps of the signals such as an appropriate baseline correction, a substantial involvement of atrial repolarization during the PQ segment can be added.

The analysis of low-level ECG potentials demands great care, as was realized right from the start of the earlier studies on P waves, the PQ segment, the ST-T segment, and the U wave.[19] The use of the RMS curve, in particular, when applied to signals referred to zero mean and supported by a spline-based baseline correction, provided a clear view of the overall timing of the depolarization and repolarization processes of the heart as observable from the ECG. This was used previously for the analysis of the low-level potentials by Mervis.[20] By comparing their defining equations, it can be seen that, apart from a scaling factor, the RMS(t) curve may be viewed as a generalization of the spatial magnitude function $M(t)$ used in vectorcardiography.

Locations of extreme potentials

During the P wave, the locations of the extreme positive and negative surface potentials were observed in regions not included in the standard 12-lead system (Fig. 2A and B).[18,20] This suggests that more optimal lead positions may be found for monitoring and analyzing atrial signals. This idea is currently investigated in our group. Preliminary results of the analysis of AF signals have corroborated this hypothesis.[21]

Approximately the same locations were identified for the extremes at $t = t_{\text{mid-PQ}}$. The locations are similar to those previously reported in the literature. We note that these locations also correspond to the efficacious positions for the application of defibrillation paddles.[22,23] This should come as no surprise in view of Helmholtz theorem of reciprocity (see, eg, Reference 24): when the electric source and the field point coordinates are interchanged, the resulting potential remains the same. To transfer electric energy to the heart with the highest efficiency, one must apply the power source at the locations where the heart's electrical activity is expressed the strongest.

The orientation of the line connecting the regions of extreme potential values, for example, those connecting the minima shown in Fig. 2A to the maxima shown in Fig. 2B, may seem to be at odds with the corresponding vector directions, for example, the one shown in Fig. 3A. This apparent discrepancy is explained by the fact that center of gravity of the atrial myocardial tissue is located at a slightly anterior position inside the thorax. This is illustrated in Fig. 5. Fig. 5A represents the body surface potentials generated by a current dipole representing the dominant vector at $t = t_{P_{\text{apex}}}$ (top row of Table 4) having the corresponding prevalent direction (second row of Table 4) located inside a homogeneous volume conductor. The thorax geometry (the same as in Fig. 2) is that of one of the subjects, derived from magnetic resonance imaging of the subject (in DB2).[4] The potential distribution was computed by using our dedicated Boundary Element Method software.[25] Note that locations of the extremes are similar to those shown in Fig. 2A and B and that the ratio of the absolute values of the extreme potentials shown in Fig. 5 is similar to what can be derived from the left column of Table 3.

Involvement of atrial repolarization

Our observations during the PQ segment confirm that although the temporal behavior of the individual signals is rather flat, a clear spatial, almost-stationary distribution is present, and hence, the PQ segment is not electrically silent.[18,20] These days, this fact is rarely acknowledged. During the Computers in Cardiology 2005 meeting in Lyon, the only presentations in which this fact can be seen came from our group (www.lausanneheart.ch). In other presentations, invariably, PQ segments coinciding with the baseline were shown, probably, but incorrectly, caused by starting the application of the baseline correction at the onset of ventricular depolarization.

The almost-reverse direction of the vector at $t = t_{\text{mid-PQ}}$ with respect to that at $t = t_{P_{\text{apex}}}$ (Fig. 3) suggests discordant atrial T waves, as do the observed locations of the extreme potentials. This in turn suggests a small dispersion of the action potential durations of atrial myocytes.[26] Usually, the PQ interval is not long enough to reach the end of atrial repolarization. However, the observations at $t = t_{\text{mid-PQ}}$, with subsequent diminishing vector magnitudes, indicated that the major expression of atrial repolarization may well be on its return at the normal timing of the onset of QRS. The results of a recent model-based analysis of atrial repolarization suggest that action potential durations of atrial myocytes are much shorter than those resulting from the commonly used Courtemanche model.[27] In fact, they are likely to be more in agreement with those of the working atrial myocardium.[28] A consequence of this would be that the ECG signals throughout the PQ interval are affected by repolarization processes.[29]

Limitations

This study was prompted during the setting up of a model aimed at supporting the analysis of ECG signals during AF. The data for the full validation of such a model are not available, and as a first step, the model was tested in an application to the normal P wave. It is here that the interest in the PQ segment arose. The signals during the PQ segment of the healthy subject studied[29] showed clear nonisoelectric potentials, and we were interested to see whether this might be due to a recording artifact. The results from the analysis of the combined data available

from 2 previous studies, as well as results from the literature are discussed. The focus here was on the quantification of magnitude of the potentials during the PQ segment of healthy subjects for which some reference data were available from the literature on body surface potential maps and VCGs. No effects of a multitude of various other possible factors or pathology were studied.

The derived model is currently used for the analysis of the simultaneous presence and superposition of atrial depolarization and atrial repolarization, or atrial repolarization and ventricular depolarization, both during normal activation and during AF. In addition, it is used to establish which chamber is contributing to which portions of atrial repolarization on the body surface. This can only be accomplished by relating the surface events to what is going on electrophysiologically in the heart at the same time. The model includes sophisticated elements for modeling the myocardial sources, linked to electrophysiology as well as of the biophysics of linking sources to body surface potentials. The results of the application of this model, extending those already shown in,[29] will be presented at a later stage.

Conclusion

This study confirms earlier reports that the PQ is not isoelectric, the time course of the potential distribution being very similar to that at the apex of the P wave but for a reversed polarity and about 3-fold lower magnitude. The local potential extremes during this segment were found at positions not sampled by the standard leads, which implies that the positions of the standard leads are suboptimal for studying the electrical activity of the atria. The results demonstrate a significant involvement of atrial repolarization during the PQ interval and essentially discordant atrial T waves, suggesting a small dispersion of atrial action potential durations. The article stresses the need for an appropriate signal processing of the (low level) atrial ECG potentials and introduces some new methods for the directional statistics of the directions involved in the analysis of vectorcardiograms.

References

1. Uijen GJH, Heringa A, van Oosterom A, van Dam RT. Body surface maps and the conventional 12-lead ECG compared by studying their performances in classification of old myocardial infarction. J Electrocardiol 1987;20/3:193.
2. Heringa A, Uijen GJH, van Dam RT. A 64-channel system for body surface potential mapping. In: Antalózcy Z, Préda I, editors. Electrocardiology 1981. Budapest: Academia Kiado; 1982. p. 297.
3. Hoekema R, Huiskamp GJM, Oostendorp TF, Uijen GHJ, van Oosterom A. Lead system transformation for pooling of body surface map data: a surface Laplacian approach. J Electrocardiol 1995;28:344.
4. Hoekema R, Uijen GJH, van Erning L, van Oosterom A. Interindividual variability of mutlilead electrocardiographic recordings: influence of heart position. J Electrocardiol 1999;32(2):137.
5. SippensGroenewegen A, Spekhorst H, Hauer RNW, van Hemel NM, Broekhuisen P, Dunning AJ. A radiotransparent carbon electrode array for body surface mapping during catheterization. Proc 9th Ann Conf IEEE-EMBS; 1987. p. 178.
6. Van Oosterom A, Hoekema R, Uijen GJH. Geometrical factors affecting the interindividual variability of the ECG and the VCG. J Electrocardiol 2000;33:S219.
7. Frank E. An accurate, clinically practical system for spatial vectorcardiography. Circulation 1956;8:737.
8. Macfarlane PW, Lawrie TDV. Diagnostic criteria. In: Macfarlane PW, Veitch Lawrie TD, editors. Comprehensive electrocardiology, vol III. Oxford: Pergamon Press; 1989. p. 1528 [Appendix 2].
9. Oostendorp TF, van Oosterom A, Huiskamp GJM. Interpolation on a triangulated 3-D surface. J Comput Phys 1989;80/2:331.
10. Mardia KV. Statistics of directional data. London: Academic Press; 1972.
11. Meisel WS. Computer-oriented approaches to pattern recognition. New York: Academic Press; 1972.
12. Poggio T, Girosi F. Network approximation and learning. Proc IEEE 1990;78/9:1481.
13. Wilson RJ. Introduction to graph theory. London: Longman; 1972.
14. Upton GJG, Fingleton B. Spatial data analysis by example. Volume 2: categorical and directional data. Chichester: John Wiley&Sons; 1989.
15. Downs TD, Liebman J. Statistical methods for vectorcardiographic directions. IEEE Trans Biomed Eng 1969;16:87.
16. Draper HW. The corrected orthogonal electrocardiogram and vectorcardiogram in 510 normal men (Frank lead system). Circulation 1964; 30:853.
17. Nemati M. The orthogonal electrocardiogram in normal women. Implications of sex differences in diagnostic electrocardiography. Am Heart J 1978;95:12.
18. d'Ambroggi L, Musso E, Taccardi B. Body-surface mapping. In: Macfarlane PW, Veitch Lawrie TD, editors. Comprehensive electrocardiology, vol II. Oxford: Pergamon Press; 1989. p. 1015 [Chapter 2].
19. Spach MS, Barr RC, Warren RB, Benson DW, Walston A, Edwards SB. Isopotential body surface mapping in subjects of all ages: emphasis on low-level potentials with analysis of the method. Circulation 1979; 59:805.
20. Mervis DM. Body surface distribution of electric potential during atrial depolarization and repolarization. Circulation 1980;62:167.
21. Ihara Z, Jacquemet V, Vesin JM, van Oosterom A. Adaptation of the standard 12-lead ECG focusing on atrial activity. Comput Cardiol 2005;203-5.
22. Heames RM. Do doctors position fibrillation paddles correctly? Observational study. BMJ 2001;322:1393.
23. Consensus report: international guidelines 2000 for CPR and ECC, part 4: the automated external defibrillator: key link in the chain of survival. Resuscitation 2000;46:73.
24. Plonsey R. Bioelectric phenomena. New York: McGraw-Hill; 1969.
25. Oostendorp TF, van Oosterom A. Source parameter estimation in inhomogeneous volume conductors of arbitrary shape. IEEE Trans Biomed Eng 1989;BME-36:382.
26. van Oosterom A. Reflections on T waves. In: Hiraoka M, editor. Advances in electrocardiology. World Scientific, Singapore; 2005. p. 807 [also available in PDF format at: www.lausanneheart.epfl.ch/publications].
27. Courtemanche M, Ramirez R, Nattel S. Ionic mechanisms underlying human atrial action potential properties: insights from a mathematical model. Am J Physiol 1998;275:H301.
28. Gelband H, Bush HL, Rosen MR, Myerburg RJ, Hoffman BF. Electrophysiologic properties of isolated preparations of human atrial myocardium. Circ Res 1972;30:293.
29. van Oosterom A, Jacquemet V. Genesis of the P wave: atrial signals as generated by the equivalent double layer source model. Europace 2005;7:S21.